# Mekanika: Majalah Ilmiah Mekanika

# Analysis of Variations in Bow Design and Vessel Speed on the Response Amplitude Operator (RAO) of a Crew Boat Using Computational Fluid Dynamics (CFD)

Arnova Chandra Cahya Kirana<sup>1</sup>, Aldias Bahatmaka<sup>1\*</sup>, Dina Malsyage<sup>1</sup>, Joung Hyung Cho<sup>2</sup>, Seo Ou Ttum<sup>3</sup>

- 1 Department of Mechanical Engineering, Universitas Negeri Semarang, Semarang, Indonesia
- 2 Interdisciplinary Program of Marine Design Convergence, Pukyong National University, Busan, South Korea
- 3 Department of Research and Development, Daewoo Shipbuilding and Marine Engineering (DSME), Geoje, South Korea

Keywords: Crew boat Bulbous bow Response amplitude operator Motion response ANSYS AQWA

## Abstract

The performance and stability of crew boats in dynamic maritime environments are significantly influenced by hull geometry, particularly the design of the bow. This study investigates the influence of various elliptical bulbous bow configurations and vessel speeds on the Response Amplitude Operator (RAO) in heave and pitch motions. Using Computational Fluid Dynamics (CFD) simulations via ANSYS AQWA, four bow configurations, including a bare hull and three bulbous bow variants, were analyzed at speeds of 6, 12, and 18 knots under regular wave conditions defined by the Joint North Sea Wave Project (JONSWAP) spectrum. To validate the accuracy and reliability of the simulation method employed in this study, a comprehensive validation procedure was undertaken. For heave motion, the RAO deviation was 3.71%, and for pitch, 4.59%, both within acceptable CFD validation standards. Results indicate a minimal impact at lower speeds; however, at 18 knots, Bow 3 achieved the most significant reduction in RAO, with reductions of up to 9% in heave and 22.4% in pitch. These findings confirm the importance of optimized bow geometry in enhancing seakeeping performance.

#### 1 Introduction

In the past decade, the demand for efficient, stable, and seaworthy support vessels such as crew boats has grown in tandem with the expansion of offshore industries, including oil, gas, and renewable energy sectors [1]. These vessels are required to operate in diverse and often harsh marine environments, making their seakeeping performance a critical design criterion. A key metric for assessing a vessel's dynamic behavior in waves is the RAO, which quantitatively describes how a ship's motion amplitude (e.g., heave, pitch, roll) responds to incident wave frequencies [2]. The magnitude and shape of RAO curves are highly sensitive to operational speed and hull geometry, particularly in the bow region, where wave structure interaction is most pronounced [2,3]. Among the most influential geometric features is the bow design, including the use of bulbous bows, axe bows, and other wave-piercing configurations.

 $\underline{https://dx.doi.org/10.20961/mekanika.v24i2.106779}$ 

Revised 17 September 2025; received in revised version 20 September 2025; Accepted 21 September 2025 Available Online 20 October 2025

2579-3144

<sup>\*</sup>Corresponding Author's email address: aldiasbahatmaka@mail.unnes.ac.id

These design choices are not merely aesthetic; they have a critical impact on wave-making resistance, pressure distribution, and flow separation along the hull [4]. For instance, bulbous bows are designed to generate counter waves that interfere destructively with bow wave systems, reducing total resistance and modifying vertical accelerations. These design elements directly influence RAO characteristics, with studies confirming that sharper or wave-piercing bows generally shift the RAO peak to higher frequencies and reduce overall motion amplitudes in specific sea states [5]. With the advancement of numerical methods, CFD has become a robust and reliable tool for evaluating these hydrodynamic effects. CFD enables detailed simulation of nonlinear wave body interactions, including viscous effects, turbulence, and transient behavior, which are difficult to capture in linear strip theory or potential flow-based methods [6].

Through CFD, it is possible to generate high-resolution data on ship motions under both regular and irregular wave conditions, across a range of speeds and sea angles. This significantly reduces reliance on costly and time-consuming towing tank experiments, making CFD not only an analytical tool but also a practical design instrument. Numerical studies using ANSYS AQWA have further explored the influence of buoy skirt geometry on motion response and Wave Current Interactions (WCI) [7]. Additionally, modifications to hull geometry, such as variations in the deadrise angle, can significantly impact both the distribution of hydrodynamic drag and the resulting wave patterns, particularly under different velocity conditions. As noted by [8], adjustments to the deadrise angle lead to changes in total resistance through their effect on the Froude number and subsequently alter wave behavior around the hull. These findings are consistent with the concept of the RAO, which emphasizes the role of hull configuration and vessel speed in determining the magnitude of a ship's motion response to wave excitation. Recent CFD-based studies have revealed consistent trends in speed-dependent RAO behavior, particularly in the heave and pitch responses [9]. At higher Froude numbers, the RAO peak amplitude increases, which implies greater dynamic loading and reduced ride comfort. This effect is especially critical for high-speed crew boats and offshore vessels operating in head or following seas. Furthermore, research has demonstrated that strategic optimization of the bulbous bow through parametric variation in volume, length, or submergence can lead to significant improvements in both resistance reduction and motion damping. These results underscore the need for integrated hydrodynamic design approaches that account for both calm water resistance and waveinduced motions under realistic operational profiles [10].

In a previous research [11], the heave and pitch movements of crew boats in relation to variations in ship speed under regular wave conditions were analyzed. The study showed that increasing the ship's speed significantly impacts the RAO values, with RAO values for pitch and heave tending to rise at certain speeds, particularly when the critical speed limit is exceeded, resulting in sailing conditions that no longer meet the comfort standards set out in NORDFORSK 1987 [12]. In this current study, the scope of investigation is extended to incorporate the role of bow geometry in influencing the RAO of the hull. Previous research has predominantly focused on the RAO analysis of the bare hull form, thereby neglecting the contribution of the bow as a critical design element. Such a limitation provides only a partial understanding of the hydrodynamic behavior, since the bow shape fundamentally governs wave interaction, added resistance, and motion response characteristics. Recognizing this gap, the present study is designed to evaluate the effects of different bow shape variations on hull RAO performance using ANSYS AQWA. By systematically comparing these configurations, this research seeks to advance the current knowledge on hull-wave interaction and provide a foundation for more optimized hull form development in future design practices.

# 2 Methodology

# 2.1 Geometry of the ship

The development of the Crew Boat model for ANSYS AQWA simulation involved a two-step software process to ensure both geometric accuracy and hydrodynamic compatibility. The initial design was created using Maxsurf CAD software. Once the model was finalized, it was exported to ANSYS Design Modeler in a compatible file format, such as STEP or IGES, to maintain geometric integrity during the transition between platforms [13].

In Design Modeler, the model underwent further optimization for hydrodynamic analysis. Unnecessary details were removed, and surface integrity was checked to eliminate errors like open edges, gaps, or self-intersection issues that would otherwise disrupt hydrodynamic mesh generation in ANSYS AQWA [13]. Maintaining a simplified yet watertight geometry ensures accurate wave structure interaction and reliable panel discretization in frequency-domain analysis. As a result of this streamlined process, an accurate Crew Boat model was created (see Figure 1 and Table 1). This model is well-suited for simulating hydrodynamic responses under various maritime conditions, ensuring that the simulations accurately reflect the vessel's operational behavior.

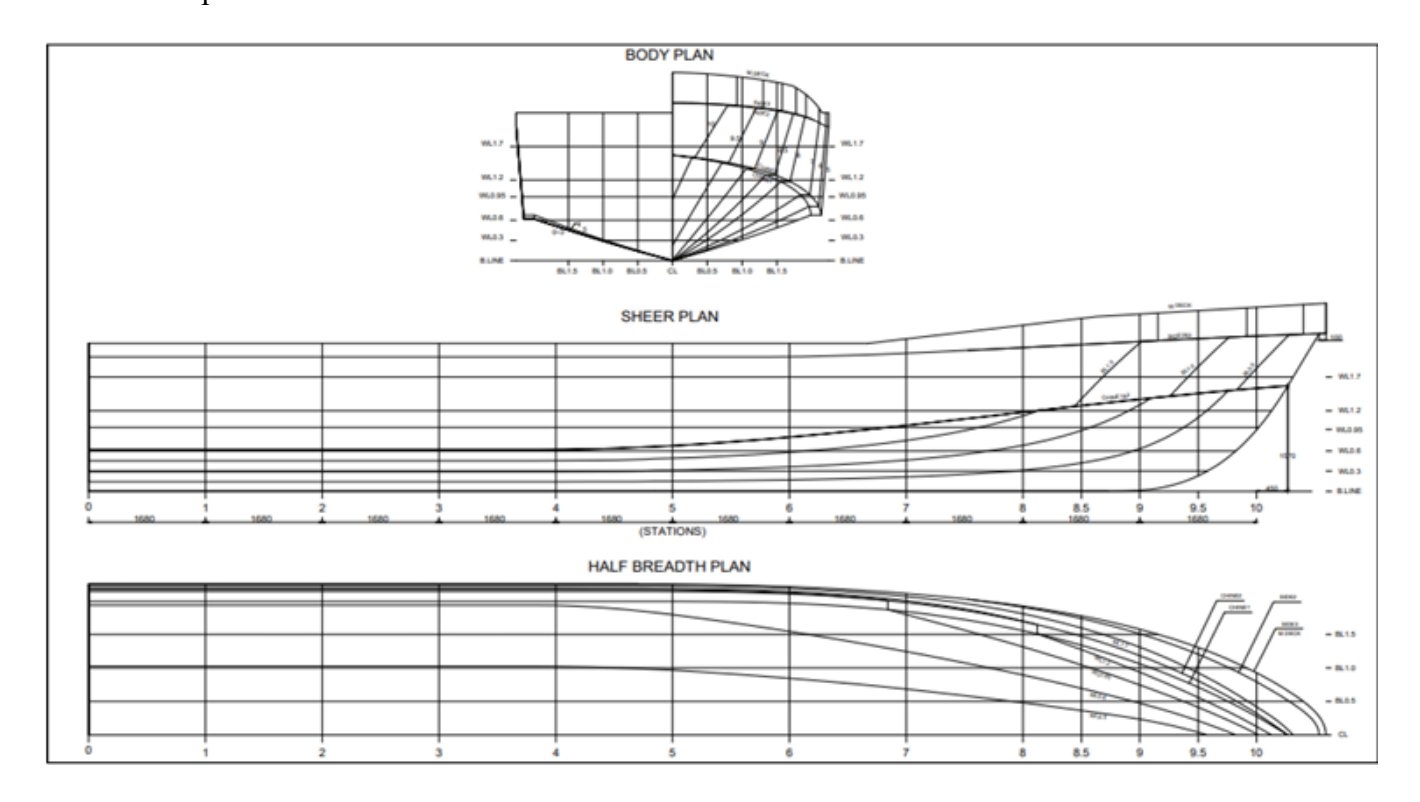


Figure 1. Line plan of crew boat type KCT 1901 [11]

**Table 1.** Primary dimension of crew boat type KCT 1901 [11]

Parameter	Boat	Unit
Length Over All (LOA)	17.800	m
Length of Waterline (LWL)	16.830	m
breadth (B)	4.500	m
draft (T)	0.950	m
displacement $(\Delta)$	36.430	ton
block coefficient (C <sub>B</sub> )	0.508	
Wetted Surface Area (WSA)	75.400	$m^2$
Longitudinal Center of Buoyancy (LCB)	6.748	m
Longitudinal Center of Floatation (LCF)	7.110	m

#### 2.2 Geometry of bulbous bow

At this stage, the design of the bulbous bow geometry was developed through the application of various modifications to the Coefficient of Bulbous Bow Width (CBB) (see Figure 2). The dimensions and proportions of each variation were meticulously determined in accordance with the parameters of the Linear Form Coefficients, ensuring a comprehensive approach to optimizing the design [14].

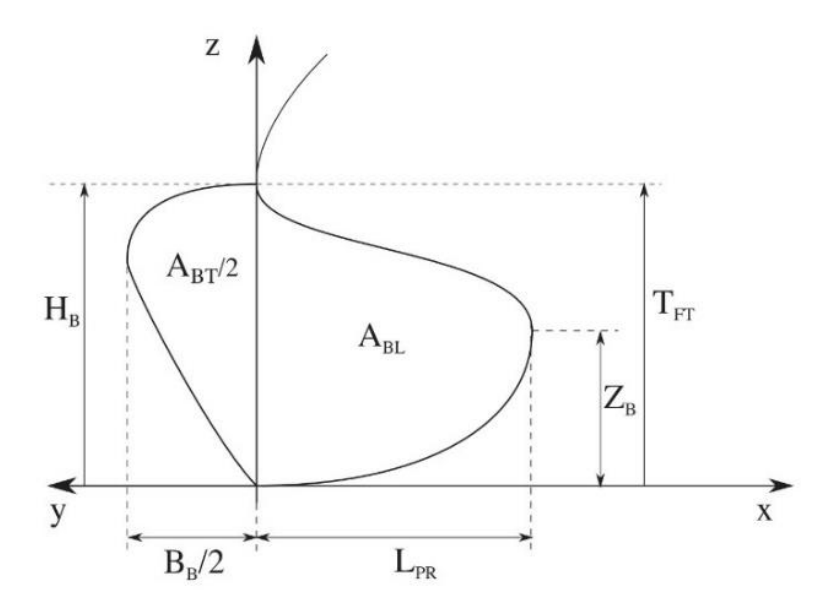


Figure 2. Geometry of bulbous bow [15]

The dimensions of the bulbous bow are determined by applying Equations 1, 2, and 3 [15].

Breadth Coefficients 
$$(C_{BB})$$
:  $\frac{B_B}{B}$  (1)

Length Coefficients 
$$(C_{LPR})$$
:  $\frac{L_{LPR}}{LPP}$  (2)

Height Coefficients 
$$(C_{ZB})$$
:  $\frac{Z_B}{T_{FT}}$  (3)

The geometric parameters of a bulbous bow are integral to its design and are typically defined in relation to specific reference points on the vessel's hull. The Length from the Fore Perpendicular (LPR) measures the extent to which the bulbous bow projects forward from the vertical reference plane at the bow. Meanwhile, the breadth at the fore perpendicular ( $B_B$ ) signifies the maximum horizontal width of the bulb at that location. Furthermore, the height of the bulbous bow from the baseline ( $Z_B$ ) indicates its vertical position in relation to the vessel's baseline, which is a critical datum in the field of naval architecture [15].

These parameters are essential for influencing the hydrodynamic efficiency of the bow, particularly in minimizing wave-making resistance and enhancing seakeeping capabilities [14,15]. By accurately configuring the LPR,  $B_B$ , and  $Z_B$ , the linear form coefficients are shown in Table 2.

**Parameter Minimum** Maximum Bow 1 Bow 2 Bow 3  $C_{BB}$ 0.17 0.20 0.17 0.185 0.20 0.018 0.031 0.018 0.0245 0.031  $C_{LPR}$  $C_{ZB}$ 0.26 0.55 0.26 0.405 0.55

**Table 2.** Linear form coefficients [15]

#### 2.3 Numerical simulation

A numerical simulation is conducted using ANSYS AQWA software. The three-dimensional (3D) model of the ship, as shown in Figure 3, is initially developed using Maxsurf Modeller. To ensure the accuracy of the simulation, a comparison of the hydrostatic data between the 3D model and the full-scale ship is presented in Table 3. Furthermore, the results of the current study are evaluated by comparing them with data from previous research. This comparison highlights the consistency and validity of the modeling approach, showing that the error gap is less than 2%, and it also identifies improvements or deviations in the current simulation results relative to established findings.



Figure 3. 3D model of crew boat type KCT 1901

**Table 3.** Comparison of the hydrostatic data

Parameter	Boat	Previous Research	Current Study	Unit	Difference (%)
Length Over All (LOA)	17.800	17.800	17.800	m	0
Length of Waterline (LWL)	16.830	16.808	16.830	m	0
breadth (B)	4.500	4.500	4.505	m	0.11
draft (T)	0.950	0.950	0.950	m	0
displacement (Δ)	36.430	36.060	36.048	ton	1.05
block coefficient $(C_B)$	0.508	0.506	0.500		1.57
Wetted Surface Area (WSA)	75.400	75.225	76.607	$m^2$	1.60
Longitudinal Center of Buoyancy (LCB)	6.748	6.768	6.806	m	0.86
Longitudinal Center of Floatation (LCF)	7.110	7.106	7.111	m	0.014

#### 2.3.1 Model crew boat and bulbous bow

In this study, an elliptical type bulbous bow was selected due to its widespread application on vessels featuring U-shaped hull forms, such as container ships and large displacement vessels [18]. This configuration is known for its effectiveness in reducing resistance and enhancing hydrodynamic efficiency at moderate to high speeds [19]. The primary function of the bulbous bow is to decrease resistance when the ship is in operation [20]. Table 4 shows the design parameters for the elliptical bulbous bow geometry. The parameters were derived using the linear form coefficient method, explicitly referencing the Coefficient of Bulbous Bow (CBB) values proposed in classical formulations by [15], which remain widely referenced in modern naval architecture [21]. As seen in Figure 4, the resulting geometric specifications are optimized to harmonize with the ship's underwater body form, ensuring minimal disturbance to the flow field and promoting improved seakeeping performance.

Table 4. Comparison of bulbous bow dimension

Parameter	Crew Boat	Bow 1	Bow 2	Bow 3
LPR	-	0.303 m	0.412 m	0,521 m
ZB	-	0.247 m	0.385 m	0.522 m
BB	-	0.765 m	0.832 m	0.900 m

This research examines the effect of various bulbous bow geometries on ship hydrodynamics by comparing four distinct configurations. The grey model represents the crew boat and serves as a reference point for evaluating performance. The first variation, Bow 1 (shown in blue), features a relatively compact design in both length and width, offering a modest enhancement in wave interaction while maintaining a streamlined shape. In Bow 2 (illustrated in red), the bow is noticeably broader and longer, enabling more efficient wave flow modulation and resistance reduction at intermediate speeds. The most substantial model, Bow 3 (depicted in yellow), incorporates the most dramatic dimensional changes, notably in height, breadth, and forward projection, and is designed for high-speed performance by optimizing water flow distribution and minimizing pitch motion. The progression from Bow 1 to Bow 3 represents a deliberate increase in size and geometric complexity to evaluate their influence on vessel dynamics. All models were assessed under consistent wave parameters and heading conditions (heading 180°), enabling a fair comparison aimed at identifying which design delivers the most significant hydrodynamic benefit [22].

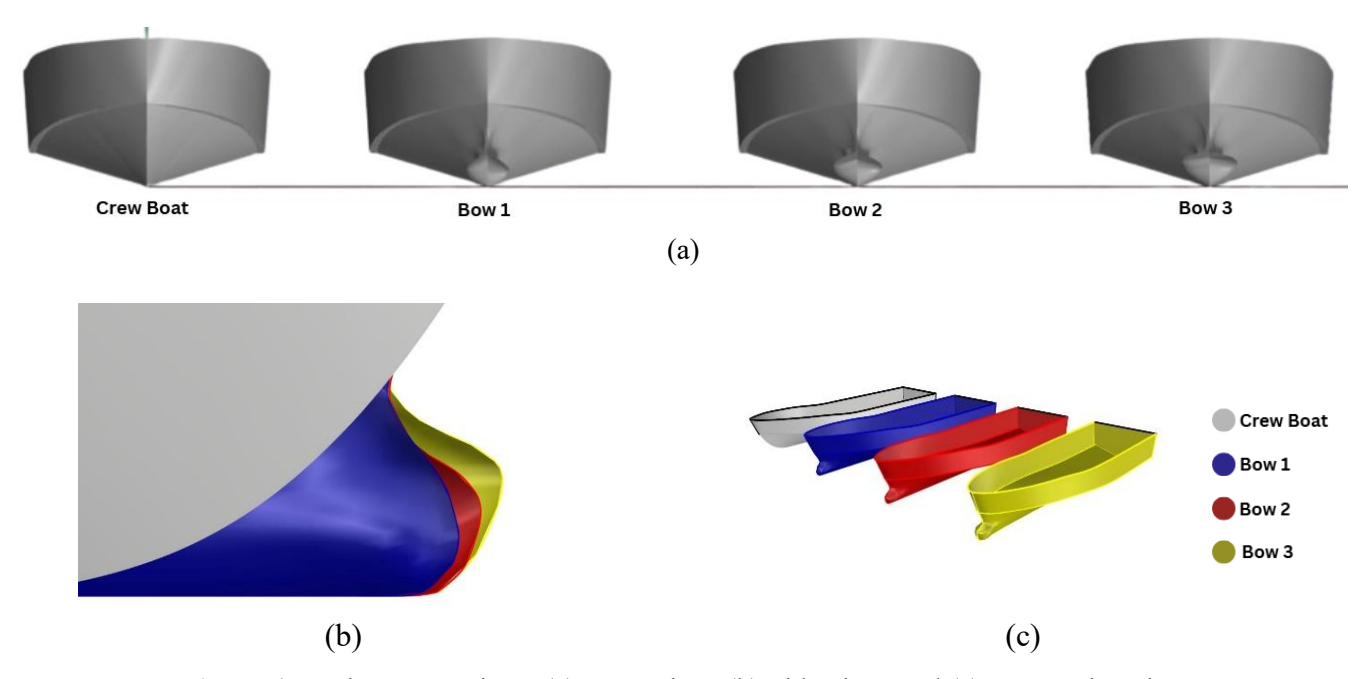


Figure 4. Design comparison: (a) Front view, (b) Side view, and (c) Perspective view

## 2.3.2 Boundary condition

In ANSYS AQWA, simulations of wave structure interactions are performed utilizing the panel method, commonly known as the Boundary Element Method (BEM). This computational approach involves breaking down the wetted surface of the ship's hull into a series of discrete panels, facilitating the resolution of potential flow problems within the frequency domain [11-19]. Each panel corresponds to a specific segment of the hull, allowing for the calculation of hydrodynamic pressures and velocities. The software interface provides extensive control over the simulation parameters, including the configuration of the sea domain specifically, water depth, wave direction, and boundary dimensions, which are designated as Water Size X, Water Size Y, and Water Level settings [11].

As mentioned in [24], the Boundary Element Method (BEM) is a widely used numerical approach in seakeeping analysis, reformulating linear partial differential equations into integral form. It defines the velocity potential (see Equation 4),

$$V = \nabla \phi = \frac{\partial \phi}{\partial x}i + \frac{\partial \phi}{\partial y}j + \frac{\partial \phi}{\partial z}k \tag{4}$$

which satisfies the Laplace equation (see Equation 5),

$$\nabla^2 \phi = 0 \tag{5}$$

under the assumptions of a homogeneous, inviscid, incompressible, irrotational, and unsteady fluid. Boundary conditions are applied, such as the body surface condition (see Equation 6),

$$\frac{\partial \phi}{\partial n} = V \cdot n \tag{6}$$

and free-surface conditions simplified to Equation 7.

$$\left(\frac{\partial^2 \zeta}{\partial t^2}\right) + g\left(\frac{\partial \phi}{\partial z}\right) = 0 \text{ at } z = 0 \tag{7}$$

By discretizing the hull into small panels, BEM captures the interaction between vessel geometry and waves, yielding the combined potential (see Equation 8).

$$\phi = \phi i + \phi r + \phi d$$
 (incident, radiation, diffraction) (8)

Pressure is obtained via the Bernoulli equation, and integrating over the wetted surface provides wave excitation forces, as implemented in AQWA software for seakeeping simulations.

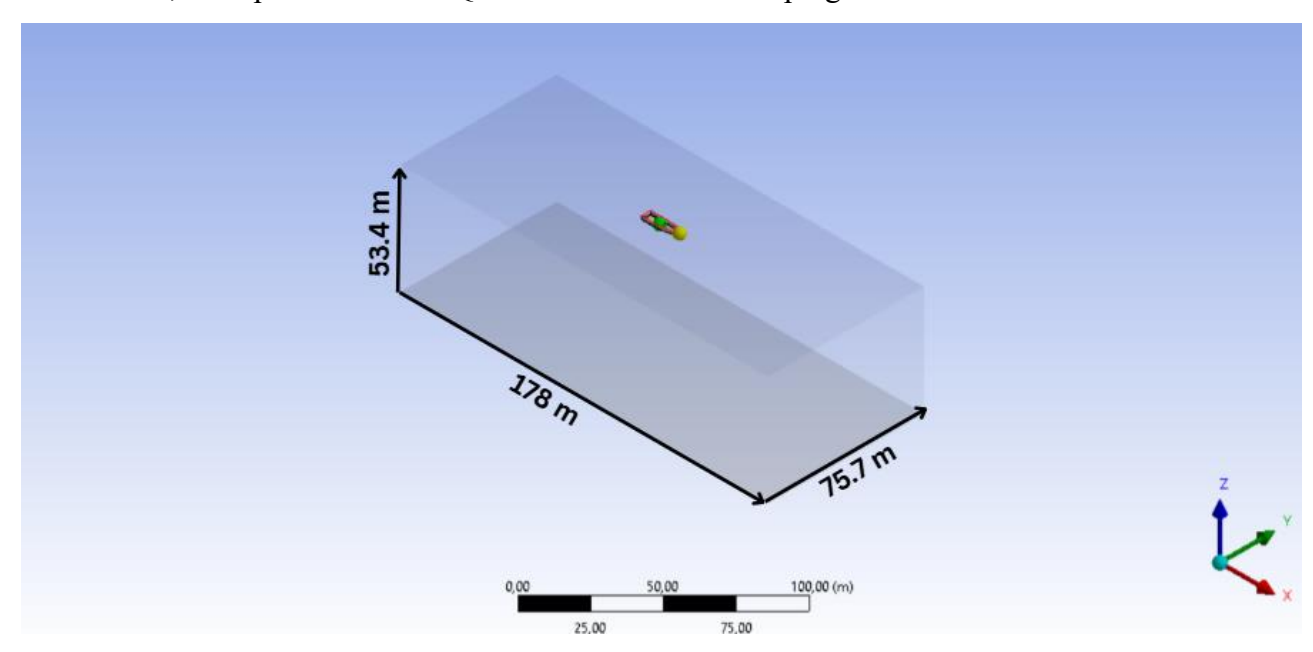


Figure 5. Computational domain used in ANSYS AQWA

Figure 5 depicts the computational domain established for this study. The dimensions of the domain extend to X = 178 meters (equivalent to ten times the overall length of the ship), Y = 75.7 meters, and Z = 53.4 meters, thereby ensuring a sufficient spatial resolution for accurately predicting wave body interactions [7-25]. The numerical simulation conducted in this study utilized ANSYS AQWA software to assess the hydrodynamic response of four different bow configurations: a baseline ship without a bow, Bulbous Bow 1, Bulbous Bow 2, and Bulbous Bow 3. All simulations were performed with a fixed heading angle of  $180^{\circ}$ , simulating the following sea conditions. Each bow configuration was analyzed at three different speeds: 6 knots, 12 knots, and 18 knots. The draft was consistently set at 0.95 meters, with a wave period of 2.58 seconds, a wave height of 0.5 meters, and a wave amplitude of 0.25 meters. These controlled conditions enable a clear comparison of how each bow design and speed affects the vessel's seakeeping performance, specifically regarding the RAO for heave and pitch responses (see Table 5).

**Table 5.** Ship's radii of gyration [26]

Component	Formula	Value (m)
$k_{xx}$	$0.34 \times \text{beam}$	1.53
$k_{vv}$	$0.25 \times length overall$	4.45
$k_{zz}$	$0.26 \times length overall$	4.628

# 2.3.3 Mesh setting

In this study, meshing plays a crucial role in ensuring the accuracy of hydrodynamic simulations. The mesh was created using the panel discretization technique, which divides the wetted surface of the vessel into smaller panels that function as source and dipole elements for fluid-structure interaction calculations. A mesh size of 0.2 meters was selected to ensure stability and optimize computational time (see Table 6). This choice is based on comparing the results obtained in the current study with those from previous research [11], which will be discussed in the following section.

	_	
Description	Value	Unit
element size	0.2	m
connection tolerance	0.1	m
maximum allowed frequency	7.866	rad/s
total nodes	10284	-
total element	10119	-

Table 6. Mesh setting and configuration

#### 2.3.4 Validation simulation method

To ensure the reliability and precision of the simulation methodologies utilized in this study, a comparative analysis was conducted alongside previous research that employed similar techniques for evaluating ship hydrodynamic responses using ANSYS AQWA, demonstrating the efficacy of panel-based methods founded on the BEM in predicting vessel motion under irregular sea conditions, especially when integrated with the JONSWAP wave spectrum [28]. Their findings underscore the critical role of appropriately configuring the simulation domain and meticulously selecting wave spectrum parameters in achieving outcomes that accurately reflect physical realities. This viewpoint is further corroborated by more recent studies, including those by [21-24], which emphasizes the importance of mesh resolution and the accuracy of wave inputs in BEM-based simulations.

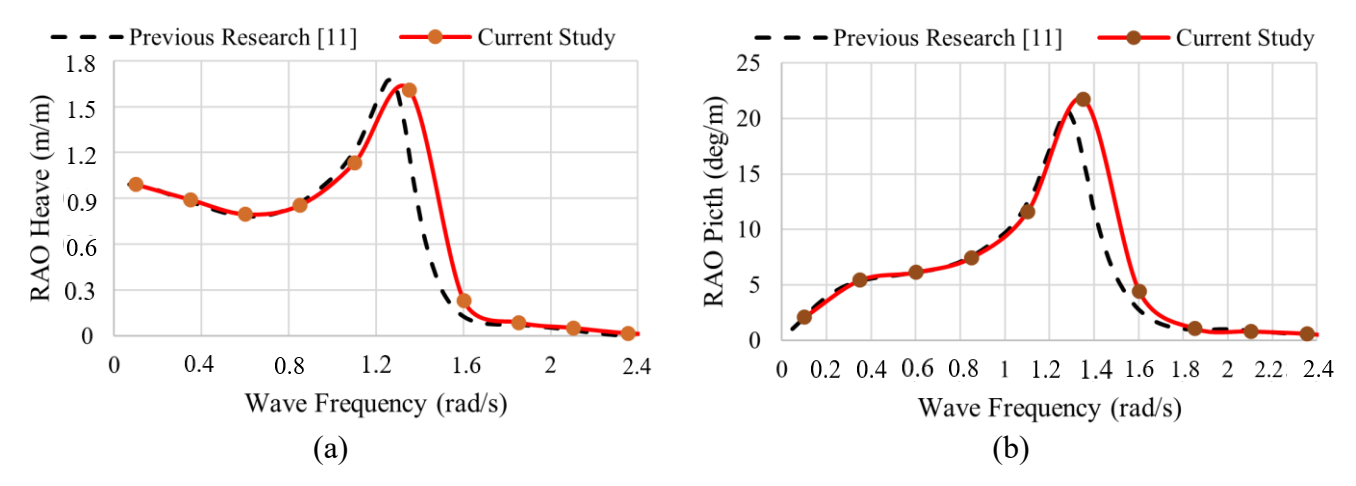


Figure 6. Comparison of RAO versus wave frequency with previous research: (a) Heave and (b) Pitch

To strengthen the robustness of this analysis, RAO values for heave and pitch were extracted under operational conditions, specifically at a vessel speed of 18 knots and a head wave angle of 180°. This condition is particularly critical for assessing a vessel's seakeeping ability [11]. These scenarios often reveal peak amplitude responses, which are vital for evaluating hull performance. The present findings confirm that the design of the bow significantly influences both vertical (heave) and rotational (pitch) motions, with optimized hull geometries leading to enhanced motion damping and improved navigational comfort. In Figure 6, to validate the accuracy and reliability of the simulation method employed in this study, a comprehensive validation procedure was undertaken.

This involved a rigorous comparison of the numerical results with both experimental observations and established numerical benchmarks. The assessment focused on two critical motion responses: heave and pitch, with RAOs evaluated at a speed of 18 knots under head sea conditions with a 180° heading angle. According to previous research (see Figure 6), the RAO for heave was documented as 1.671 m/m. In contrast, the current study produced a value of 1.609 m/m, resulting in a relative deviation of 3.71%. In terms of pitch motion, the previous research reported a RAO of 20.752 degrees/m, in contrast to the current study's finding of 21.705 degrees/m, which reflects an error margin of 4.59%.

These deviation levels are within the generally accepted thresholds for CFD based seakeeping validation and corroborate the standards found in previous literature [19,21-24]. The minimal discrepancies observed support the assertion that the current numerical model aligns closely with empirically validated outcomes, thereby reinforcing the robustness and reliability of the simulation methodology employed. It can be verified by comparing simulation results with error gaps of less than 5% [30].

#### 2.4 Wave condition

JONSWAP spectrum is a widely used wave spectral model that originates from empirical observations made in the North Sea, where wind-driven conditions strongly influence wave behavior [31]. It provides a refined description of sea states that are fetch-limited and still undergoing development, distinguishing it from the fully developed Pierson-Moskowitz spectrum. This spectrum is especially effective in characterizing young seas, where wave energy concentration is higher around the peak frequency, allowing for a more realistic representation of wave dynamics under transitional wind conditions. In the context of hydrodynamic simulations using ANSYS AQWA, the JONSWAP spectrum is implemented to model random wave environments, which in turn facilitates the prediction of vessel or offshore structure responses under irregular sea states [11-27].

These simulations capture motion responses across heave and pitch, also assessing wave structure interactions, including radiation and diffraction forces. The mathematical formulation of the JONSWAP spectrum, defined by its spectral density function, incorporates a peak enhancement factor ( $\gamma$ ) that amplifies the energy near the peak frequency, improving the accuracy of RAO estimations for floating bodies. Equation 9 defines the JONSWAP spectrum.

$$S\zeta(\omega) = \propto g^2 \omega^{-5} \exp\left\{-1.25 \left(\frac{\omega}{\omega_0}\right)^{-4}\right\} \gamma^{\exp\left\{-\frac{(\omega - \omega_0)}{2\tau \omega_0^2}\right\}}$$
(9)

# 2.5 Response amplitude operator

RAOs are mathematical tools that describe how a ship responds to ocean waves. Specifically, RAOs represent the relationship between the amplitude of a ship's response and the amplitude of incoming waves [33]. They quantify the dynamic behavior of a structure in response to waves across a specified frequency spectrum. By using RAOs, one can convert wave forces into the corresponding dynamic responses of the structure, often represented through Equation 10 [34].

$$RAO(\omega_e) = \frac{X_p(\omega_e)}{\mu_\omega(\omega_e)}$$
(10)

where  $X_p(\omega_e)$  is the amplitude of motion and  $\mu_{\omega}(\omega_e)$  is the amplitude of the wave.

# 2.6 Response spectra

The response spectrum is calculated by combining the RAO with the wave spectrum, as presented in Equation 11 [35].

$$S_{\zeta r}(\omega_e) = [RAO(\omega_e)]^2 S_{\zeta}(\omega_e)$$
(11)

where  $S_{\zeta r}(\omega_e)$  is the response spectrum, RAO $(\omega_e)$  is a transfer function, and  $S_{\zeta}(\omega_e)$  is a wave spectrum.

Based on the CFD simulation with regular waves, the bow exhibits a motion response. The spectral density of this relative bow motion can be determined using Equation 12 [35].

$$S_s(\omega_e) = S_z \frac{\pi L}{L_w} S_\theta - S_\zeta \tag{12}$$

In this equation,  $S_s(\omega_e)$  denotes the spectral density of the relative bow motion,  $S_z$  represents the spectral density response spectrum for heave,  $S_\theta$  represents the spectral density response spectrum for pitch,  $S_\zeta$  is the spectral density of the wave spectrum, L is the distance from the ship's Center of Gravity (CG), and  $L_w$  is the wavelength. Based on the spectral density of the relative bow motion, the vertical velocity and vertical acceleration spectra can be derived using the formulas given in Equations 13 and 14 [35].

$$S_v(\omega_e) = \omega_e^2 S_{\zeta r}(\omega_e) \tag{13}$$

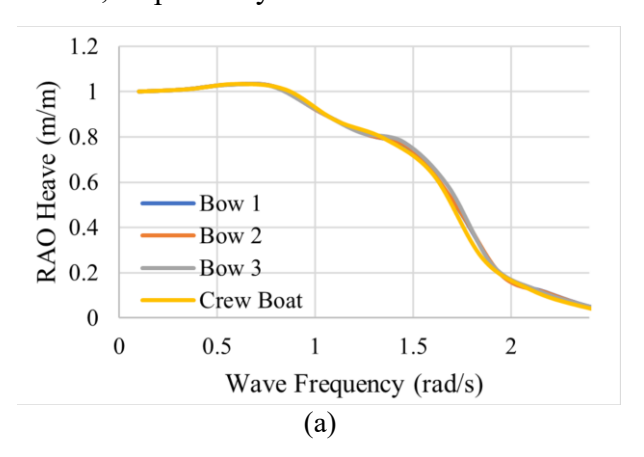
$$S_a(\omega_e) = \omega_e^4 S_{\zeta r}(\omega_e) \tag{14}$$

Here,  $S_v$  denotes the vertical velocity spectrum and  $S_a$  denotes the vertical acceleration spectrum as response statistics. The Root Mean Square (RMS) and the significant amplitudes of these responses are then calculated as one of the seakeeping criteria, following NORDFORSK in 1987. The RMS value is determined as  $\sqrt{m_n}$ , while the significant amplitude is expressed as  $2\sqrt{m_n}$ , where  $\sqrt{m_n}$  represents the area under the spectral curve.

#### 3 Results and Discussion

#### 3.1 Results of RAO simulation based on the frequency domain

The CFD software serves as a valuable tool in analyzing seakeeping performance. The initial input data encompasses variations in both speed and wave periods. The results generated include RAO graphs, alongside graphical representations of the ship's heave and pitch motion elevations. The findings from the CFD analysis are presented in Figure 7. As vessel speed increases to 12 knots, the disparities in RAO Heave and RAO Pitch values become more pronounced. The highest RAO Pitch is observed with Bow 3 at 18.721 degrees per meter, followed by Bow 1 at 18.307 degrees per meter and Bow 2 at 18.227 degrees per meter. In contrast, the vessel without a bow records the lowest RAO Pitch at 16.616 degrees per meter. For RAO Heave, the ship without a bow measures 1.143 m/m, while both Bow 1 and Bow 2 present values of 1.112 m/m. Bow 3 exhibits the highest RAO Heave among the designs, with a value of 1.185 m/m. At a speed of 18 knots, both RAO Heave and RAO Pitch values increase significantly. The vessel without a bow has the highest RAO Heave at 1.609 m/m, followed by Bow 2 at 1.549 m/m, Bow 1 at 1.529 m/m, and Bow 3 at 1.466 m/m. For RAO Pitch, the vessel without a bow also leads at 21.705 degrees per meter, while Bow 3 has the lowest at 16.844 degrees per meter. Bow 1 and Bow 2 have values of 18.251 and 18.513 degrees per meter, respectively.



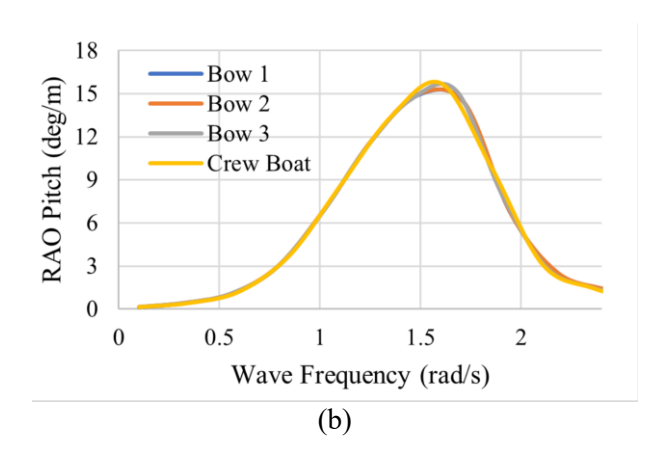


**Figure 7.** Variations RAO of Speed: (a) Heave 6 knots, (b) Pitch 6 knots, (c) Heave 12 knots, (d) Pitch 12 knots, (e) Heave 18 knots, and (f) Pitch 18 knots

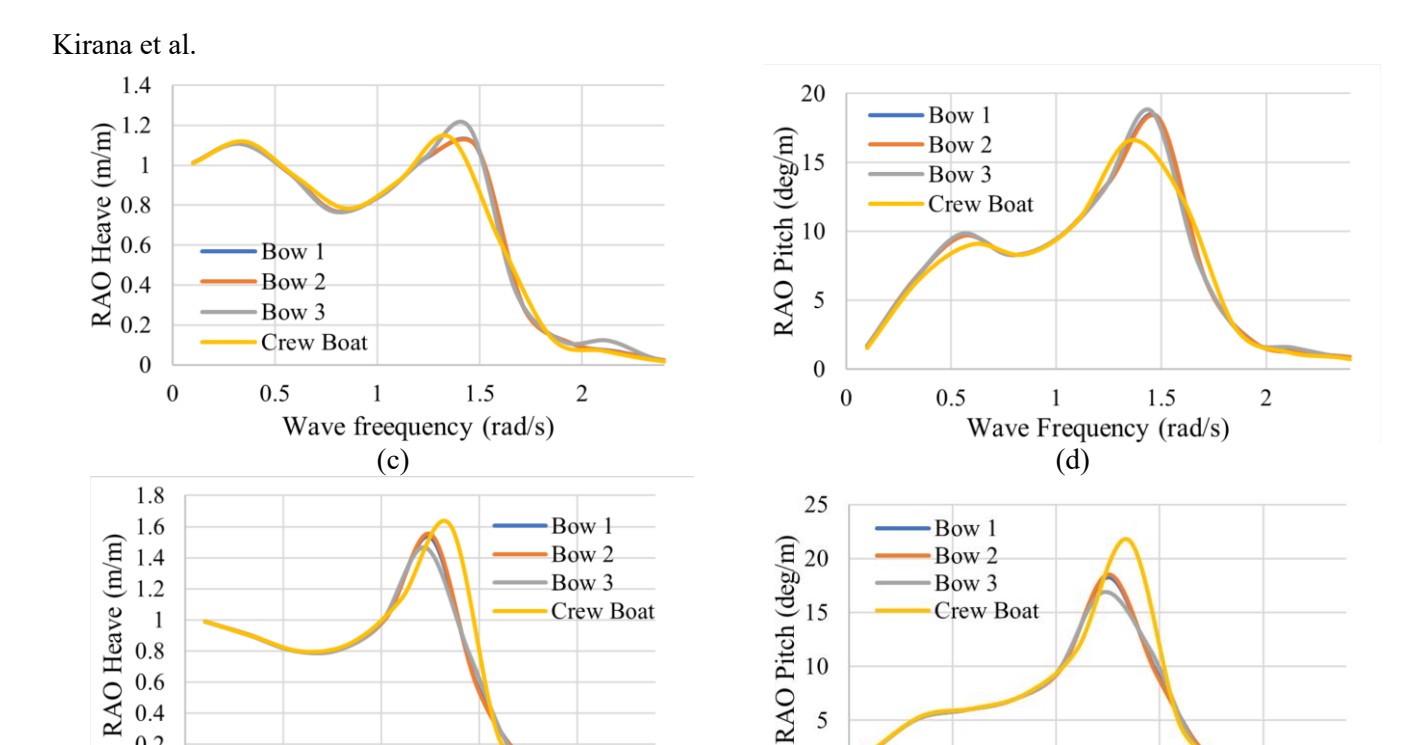


Figure 7. Cont.

10

5

0

0

0.5

1

(f)

Wave Frequency (rad/s)

1.5

2

At 6 knots, the vessel without a bow still has the highest RAO Heave at 1.035 m/m, closely followed by Bow 1 and Bow 2 at 1.032 m/m, and Bow 3 at 1.030 m/m. For RAO Pitch, Bow 1 performs best at 14.888 deg/m, but the vessel without a bow records a higher value at 15.700 deg/m. At 12 knots, the ship without a bow's RAO Heave rises to 1.143 m/m, while Bow 1 and Bow 2 drop to 1.112 m/m. Bow 3 increases to 1.185 m/m. In the RAO Pitch, Bow 3 achieves the highest at 18.721 deg/m, while the vessel without a bow has the lowest at 16.616 deg/m. The most significant differences occur at 18 knots, where the ship without a bow shows a RAO Heave of 1.609 m/m and RAO Pitch of 21.705 deg/m. Bow 3 performs best with the lowest values at 1.466 m/m for RAO Heave and 16.844 deg/m for RAO Pitch. This illustrates the importance of bow design at higher speeds.

# 3.2 Contour of crew boat and variations of bulbous bow response to waves

0.8

0.6 0.4

0.2

0

0

0.5

1

Wave Frequency (rad/s) (e)

1.5

2

This section delves into wave elevation contour plots, exemplified by Figure 8, which provide critical spatial representations of the interactions between waves and a vessel's hull. These contour plots depict the distribution of wave surface elevation surrounding the ship, typically expressed in angular frequency (rad/s). Such visualizations are paramount for elucidating the phenomena of wave reflection, diffraction, and radiation induced by the presence of the vessel. The color gradients within the contour plots signify varying intensities of wave elevation: regions denoted in red indicate areas where the ship experiences the highest wave crests. At the same time, blue zones represent troughs or regions of minimal wave impact. This graphical interpretation significantly contributes to our understanding of wave structure interactions, which directly influence the vessel's motions, including heave, pitch, and roll. Moreover, contour plots serve a critical function in validating the precision of numerical hydrodynamic simulations, facilitating the accurate definition of panel mesh and boundary conditions. The simulation results provide comprehensive insights into the hydrodynamic behavior of vessels with varying bow configurations, including Crew Boat, Bow 1, Bow 2, and Bow 3, under regular wave conditions using ANSYS AQWA. For the Crew Boat, the wave surface elevation contour indicates a wave frequency of 0.85153 rad/s, an amplitude of 0.25 meters, and a direction of 180°, corresponding to a following sea condition.

The wave elevation ranged from +2.96091 m (crest) to -2.96091 m (trough), with pronounced disturbances around the hull edges due to wave diffraction. Correspondingly, the structure motion amplitude contour reveals vertical displacements ranging from 0.0008 m to 0.38674 m, peaking near the stern. This highlights the vessel's vulnerability to wave-induced motions such as heave and pitch in the absence of a bow design. These results serve as a performance baseline for assessing alternative bow geometries. Introducing Bow 1 resulted in noticeable improvements. The structural motion amplitude ranged from 0.00156 m to 0.31785 m, with reduced motion mainly in the midship and bow areas, suggesting enhanced dynamic stability. The wave surface elevation was more evenly distributed, ranging from +0.37564 m to -0.37564 m, with a smoother, more symmetrical pattern around the hull. This indicates that Bow 1 effectively managed wave energy distribution, particularly around the bow, reducing wave build-up compared to the bare hull. The Bow 2 configuration exhibited similar performance trends with a structural motion amplitude ranging from 0.00173 m to 0.31759 m, again concentrated toward the stern but slightly less effective than Bow 1 in minimizing overall displacement. The surrounding wave field showed elevation values from +0.36737 m to -0.36737 m, maintaining a relatively symmetrical and smooth pattern. While Bow 2 contributed to energy diffusion, its impact on reducing surface disturbances was slightly less significant than that of Bow 1. This suggests a moderate improvement over the base design, but not optimal in suppressing vertical motions.

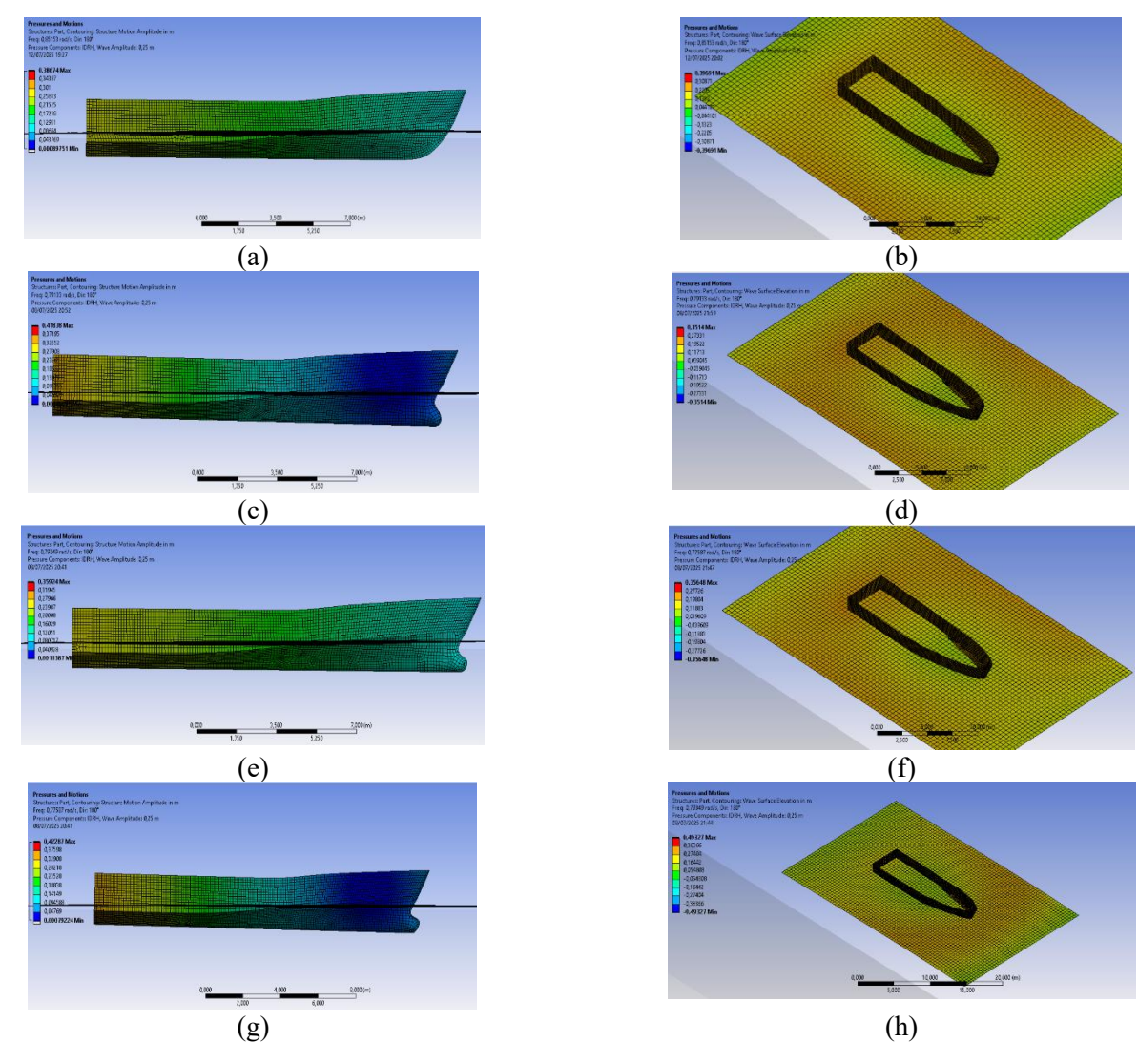


**Figure 8.** Motion results in CFD: (a) Motion amplitude crew boat, (b) Wave elevation crew boat, (c) Motion amplitude bow 1, (d) Wave elevation bow 1, (e) Motion amplitude bow 2, (f) Wave elevation bow 2, (g) Motion amplitude bow 3, and (h) Wave elevation bow 3

Finally, Bow 3 exhibited the optimal hydrodynamic performance among all configurations tested. The structural motion amplitude ranged from 0.00274 m to 0.29784 m, indicating the lowest maximum displacement among all designs and demonstrating superior control of heave and pitch, particularly near the stern. The wave surface elevation values ranged from +0.37564 m to -0.37564 m, and the wave field surrounding the hull displayed a well-dispersed, stable contour with minimal fluctuations near the bow. This suggests that Bow 3 most effectively redirected wave flow around the hull, minimizing diffraction and reducing hydrodynamic loading on the structure. Notably, the comparative analysis across the four configurations underscores the significant impact of bow design on a vessel's seakeeping ability. Bow 3 emerged as the most efficient design, offering the best performance in reducing motion amplitudes and managing wave interactions, followed by Bow 1 and Bow 2. In contrast, the vessel without a bow exhibited the highest wave-induced motion responses. These findings reinforce the importance of optimizing bow geometry to enhance vessel stability and hydrodynamic efficiency under the following sea conditions.

#### **4 Conclusions**

All three bow design variations demonstrated a significant influence in reducing RAO Heave and RAO Pitch, with Bow 3 showing the most effective performance by decreasing the RAO values by approximately 9% and 22.4%, respectively, compared to the vessel without a bow. while the effects of bow design may be less pronounced at lower speeds, they become increasingly significant as vessel speed rises. Among the configurations evaluated, Bow 3 demonstrates superior hydrodynamic characteristics, effectively minimizing both heave and pitch responses. This makes Bow 3 the most advantageous design for enhancing vessel stability and seakeeping performance under dynamic maritime conditions.

The results of the simulation clearly demonstrate that bow design has a significant influence on the hydrodynamic performance and motion response of a vessel under wave excitation, particularly in following sea conditions. Among the four configurations tested, the ship without a bow exhibited the highest motion amplitudes and the most severe wave surface disturbances, making it the least effective in mitigating heave and pitch. The introduction of Bow 1 and Bow 2 showed noticeable improvements, with Bow 1 slightly outperforming Bow 2 in reducing structural displacement and distributing wave energy more symmetrically. However, it is the Bow 3 configuration that delivered the best overall performance, achieving the lowest vertical motion amplitudes and the smoothest wave elevation contour around the hull. This indicates that Bow 3 is the most effective design in minimizing wave-induced motions and improving seakeeping behavior. Therefore, Bow 3 can be considered the optimal solution for enhancing vessel stability and reducing hydrodynamic loads under regular wave conditions. Future research is recommended to explore the influence of irregular sea states and oblique wave angles, and to incorporate nonlinear time-domain analysis, which will better reflect real operational conditions.

# 5 Acknowledgement

The author gratefully acknowledges the support provided by the Department of Mechanical Engineering, Universitas Negeri Semarang, in facilitating the research titled "Analysis of the Effects of Bow Design Variations and Vessel Speed on the RAO of a Crew Boat Using CFD". This support has been instrumental from the Faculty of Engineering with Contract Number: 139.03.2.693449/2025.05/2025, Universitas Negeri Semarang.

# References

- 1. O. V. Zakharchenko, D. I. Bedrii, O. V. Bileha, O. Y. Savina, and O. V. Haidaienko, "Crewing of Sea Vessels Taking into Account Project Risks and Technical Condition of Ship Equipment," *J. Rev. Glob. Econ.*, vol. 9, pp. 130-140, 2020.
- 2. M. R. Davis, N. L. Watson, and D. S. Holloway, "Measurement of Response Amplitude Operators for an 86 m High-Speed Catamaran," *J. Ship Res.*, vol. 49, no. 2, pp. 121-143, 2005.
- 3. M. G. Chiţu, R. Zăgan, and E. Manea, "Analysis for the amplitude oscillatory movements of the ship in response to the incidence wave," *IOP Conf. Ser. Mater. Sci. Eng.*, vol. 95, no. 1, article no. 012076, 2015.

- 4. M. K. Sanchana, R. Vijayakumar, and V. V. S. Prasad, "Design Approach for Reducing the Wave Added Resistance by Hull Form Optimisation," *Lect. Notes Civ. Eng.*, vol. 22, pp. 385-400, 2019.
- 5. R. Sharma and O. P. Sha, "Hydrodynamic Design of Integrated Bulbous Bowlsonar Dome for Naval Ships," *Def. Sci. J.*, vol. 55, no. 1, pp. 21-36, 2005.
- 6. J. Westphalen, D. M. Greaves, A. Raby, Z. Z. Hu, D. M. Causon, C. G. Mingham, P. Omidvar, P. K. Stansby, B. D. Rogers, J. Westphalen, D. M. Greaves, A. Raby, Z. Z. Hu, D. M. Causon, C. G. Mingham, P. Omidvar, P. K. Stansby, and B. D. Rogers, "Investigation of Wave-Structure Interaction Using State of the Art CFD Techniques," *Open J. Fluid Dyn.*, vol. 4, no. 1, pp. 18-43, 2014.
- 7. T. Gaggero, F. Bucciarelli, G. Besio, A. Mazzino, and D. Villa, "A method to assess safety and comfort for different ships types in a region of interest," *Ocean Eng.*, vol. 250, article no. 110995, 2022.
- 8. A. Bahatmaka, M. Y. Wibowo, A. A. Ghyfery, M. Harits, S. Anis, D. F. Fitriyana, R. F. Naryanto, A. Setiyawan, R. Setiadi, A. R. Prabowo, and K. D. Joon, "Numerical Approach of Fishing Vessel Hull Form to Measure Resistance Profile and Wave Pattern of Mono-Hull Design," *J. Adv. Res. Fluid Mech. Therm. Sci.*, vol. 104, no. 1, pp. 1-11, 2023.
- 9. P. O. Vangbo, *CFD in Conceptual Ship Design*, Trondheim: Norwegian University of Science and Technology, 2011.
- 10. Y. Lu, X. Chang, and A. kang Hu, "A hydrodynamic optimization design methodology for a ship bulbous bow under multiple operating conditions," *Eng. Appl. Comput. Fluid Mech.*, vol. 10, no. 1, pp. 330-345, 2016.
- 11. A. I. Wulandari, I. K. A. P. Utama, A. Rofidayanti, and D. Hudson, "A hydrodynamic optimization design methodology for a ship bulbous bow under multiple operating conditions," *CFD Lett.*, vol. 16, no. 4, pp. 1-15, 2024.
- 12. Jamal, A. Sulisetyono, and W. D. Aryawan, "Review of the seakeeping criteria for the study of a passenger ship criteria in Indonesian water," *IOP Conf. Ser. Mater. Sci. Eng.*, vol. 982, no. 1, article no. 012041, 2020.
- 13. ANSYS, "ANSYS AQWA user manual." ANSYS Inc, 2022.
- 14. Kiryanto, D. Chrismianto, E. S. Hadi, and A. Firdhaus, "Study of the effect on the addition of anti-slamming bulbous bow to total resistance in tugging supply vessel using CFD," *IOP Conf. Ser. Earth Environ. Sci.*, vol. 698, no. 1, article no. 012007, 2021.
- 15. A. M. Kracht, "Design of Bulbous Bows," *SNAME Trans.*, vol. 86, pp. 197-217, 1978.
- 16. M. Javadi, M. D. Manshadi, S. Kheradmand, and M. Moonesun, "Experimental investigation of the effect of bow profiles on resistance of an underwater vehicle in free surface motion," *J. Mar. Sci. Appl.*, vol. 14, no. 1, pp. 53-60, 2015.
- 17. W. Seok, G. H. Kim, J. Seo, and S. H. Rhee, "Application of the Design of Experiments and Computational Fluid Dynamics to Bow Design Improvement," *J. Mar. Sci. Eng.*, vol. 7, no. 7, article no. 226, 2019.
- 18. T. G. Tran, C. V. Huynh, and H. C. Kim, "Optimal design method of bulbous bow for fishing vessels," *Int. J. Nav. Archit. Ocean Eng.*, vol. 13, pp. 858-876, 2021.
- 19. M. A. Budiyanto, M. A. Murdianto, and M. F. Syahrudin, "Study on the Resistance Reduction on High-Speed Vessel by Application of Stern Foil Using CFD Simulation," *CFD Lett.*, vol. 12, no. 4, pp. 35-42, 2020.
- 20. Samuel, D. J. Kim, M. Iqbal, A. Bahatmaka, and A. R. Prabowo, "Bulbous bow applications on a catamaran fishing vessel for improving performance," *MATEC Web Conf.*, vol. 159, article no. 02057, 2018.
- 21. K. T. Waskito and Yanuar, "On the High-Performance Hydrodynamics Design of a Trimaran Fishing Vessel," *J. Adv. Res. Fluid Mech. Therm. Sci.*, vol. 83, no. 1, pp. 17-33, 2021.
- 22. S. Zhang, Q. Wu, J. Liu, S. Li, and H. Yasukawa, "Impact of bulbous bow shapes on hydrodynamic derivatives due to hybrid drifting and circular motion tests," *Ocean Eng.*, vol. 289, article no. 116182, 2023.
- 23. S. Tavakoli, R. N. Bilandi, S. Mancini, F. De Luca, and A. Dashtimanesh, "Dynamic of a planing hull in regular waves: Comparison of experimental, numerical and mathematical methods," *Ocean Eng.*, vol. 217, article no. 107959, 2020.
- 24. A. I. Wulandari, A. Sulisetyono, I. K. A. P. Utama, B. Ali, P. Virliani, E. Arianti, Nurhadi, M. A. Mudhoffar, A. K. Arifah, and H. Zen, "Seakeeping Performance of Warship Catamaran under Varied Hull Separation and Wave Heading Conditions," *Pomorstvo*, vol. 38, no. 2, pp. 275-296, 2024.
- 25. T. Tezdogan, A. Incecik, and O. Turan, "Operability assessment of high speed passenger ships based on human comfort criteria," *Ocean Eng.*, vol. 89, pp. 32-52, 2014.
- 26. ANSYS AQWA, Workshop 2.1 ANSYS Aqwa Hydrodynamic Diffraction, Pennsylvania: ANSYS Inc., 2013.
- 27. K. Maki, F. Zhao, P. Horn, J. Banks, J. Martio, B. Starke, S. Zaghi, D. Villa, M. Vitola, H. S. Yoon, Y. Jiang, and S. Shingo, "ITTC Quality System Manual Recommended Procedures and Guidelines: Uncertainty Analysis in CFD Verification and Validation, Methodology and Procedures," in the *International Towing Tank Conference*, Tasmania, Australia, 2024.

- 28. R. H. M. Huijsmans, R. Van 't Veer, and M. Kashiwagi, "Ship Motion Predictions: A Comparison Between a CFD Based Method, a Panel Method and Measurements," *Proc. Int. Conf. Offshore Mech. Arct. Eng. OMAE*, vol. 3, pp. 685-691, 2010.
- 29. C. C. Fang and H. S. Chan, "An investigation on the vertical motion sickness characteristics of a high-speed catamaran ferry," *Ocean Eng.*, vol. 34, no. 14-15, pp. 1909-1917, 2007.
- 30. A. Bahatmaka, D. F. Fitriyana, S. Anis, A. Y. Maulana, M. Tamamadin, S. W. Lee, and J. H. Cho, "Analytical Review of Numerical Analysis in Hydrodynamic Performance of the Ship: Effect to Hull-Form Modifications," *Mekanika Majalah Ilmiah Mekanika*, vol. 23, no. 1, pp. 54-63, 2024.
- 31. J. Staneva, V. Alari, Ø. Breivik, J. R. Bidlot, and K. Mogensen, "Effects of wave-induced forcing on a circulation model of the North Sea," *Ocean Dyn.*, vol. 67, no. 1, pp. 81-101, 2017.
- 32. E. B. Djatmiko, *Behavior and operability of marine structures on random waves*, Surabaya: ITS Press, 2012. (In Indonesian)
- 33. M. A. Lutfi, A. R. Prabowo, E. M. Muslimy, T. Muttaqie, N. Muhayat, H. Diatmaja, Q. T. Do, S. J. Baek, and A. Bahatmaka, "Leisure Boat Concept Design: Study on the Influence of Hull Form and Dimension to Increase Hydrodynamic Performance," *Int. J. Mech. Eng. Robot. Res.*, vol. 13, no. 1, pp. 139-161, 2024.
- 34. Shanty, H. Supomo, and S. Nugroho, "Analysis of crew competence factor in the ship collisions (Case study: Collision accident in Indonesian waters)," *IOP Conf. Ser. Earth Environ. Sci.*, vol. 557, no. 1, article no. 012047, 2020.
- 35. R. Bhattacharyya, *Dynamics of Marine Vehicles*. New Jersey: John Wiley & Sons Inc, 1978.